Proceedings of the Seventh International Conference on
Railway Technology: Research, Development and Maintenance
Edited by: J. Pombo
Civil-Comp Conferences, Volume 15, Paper 9.6
Civil-Comp Press, Edinburgh, United Kingdom, 2026
ISSN: 2753-3239, doi: 10.4203/ccc.15.9.6

A Resilience-Based Metric Framework for Quantifying Dynamic Wheel–Rail Adhesion Recovery

T. Wang[1,2], W. Wang[1,3], J. Ding[1,2] and J. Zuo[1,2]

[1] College of Transportation, Tongji University, Shanghai, China
[2] Shanghai Key Laboratory of Rail Infrastructure Durability and System Safety, Tongji University, China
[3] National Maglev Transportation Engineering R&D Center, Tongji University, Shanghai, China

Abstract

Low wheel-rail adhesion is a braking-safety concern because the maximum usable adhesion coefficient may be insufficient and its recovery after contamination or adhesion-enhancement intervention can be highly transient. This paper proposes an adhesion-resilience metric framework for quantifying degradation, lag, recovery and post-recovery steady behaviour. Dimensionless indices for robustness, recovery ability, adhesion utilisation efficiency, recovery rate, recovery intensity and temporal response are combined into an integrated adhesion-resilience index. Digitised rolling-contact curves from two published case groups, wet-contact sanding and oil-contamination tests, are re-analysed. Because the source curves use cycles as the horizontal coordinate, a generalised process coordinate is adopted. The results show that the proposed metrics provide information beyond maximum adhesion and support low-adhesion braking-safety assessment.

Keywords: wheel–rail adhesion, resilience metric, braking safety, low adhesion, adhesion recovery, sanding

1 Introduction

Wheel–rail adhesion directly constrains the transfer of traction and braking forces. Classical rolling-contact theory provides the theoretical basis for relating creepage, tangential force and the available adhesion level in the contact patch [1]. For traction or braking operation close to the adhesion limit, creep-force models must also represent the nonlinear saturation and possible post-peak behaviour of the adhesion–creep relationship [2]. From a tribological perspective, the wheel–rail interface is an open rolling–sliding contact in which adhesion, wear and particle generation are coupled rather than independent phenomena [3]. This coupling is particularly important for braking safety, because the same intervention that increases adhesion may also modify surface damage, wear, electrical contact and subsequent adhesion evolution.

Low adhesion is primarily induced by third-body contamination and adverse environmental conditions. Water has long been recognised as a dominant factor in wheel–rail adhesion degradation [4]; leaf films and leaf-derived layers can further produce severe low-adhesion states, which has motivated extensive laboratory testing of friction modifiers and adhesion enhancers in leaf-contaminated contacts [5]. Previous wheel–rail rolling-contact research reported that small quantities of water, oil or leaf contamination can reduce adhesion to low-adhesion levels and that the duration of the low-adhesion state increases with contaminant quantity [6]. These findings indicate that low adhesion should not be treated only as a static reduction in the maximum coefficient, but also as a transient process with a finite degradation and recovery history.

Sanding is the most common operational measure for recovering adhesion under contaminated conditions. Reviews of sanding-system research show that particles are widely used to restore adhesion and remove leaf layers, but that sand delivery, entrainment, particle characteristics and application rate strongly influence the actual contact response [7]. Laboratory studies on friction modifiers in dry, wet and leaf-contaminated wheel–rail contacts further show that adhesion restoration depends on the contact state, slip level and the solid components of the applied material [5, 8]. At the same time, dry-contact sanding may cause lubricity and electrical insulation problems when excessive sand forms a compacted insulating layer [9], and sanding can increase wear at the wheel–rail interface [10]. Scaled twin-disc tests with a real sanding system have demonstrated that sand quantity, slip and rolling speed all affect adhesion recovery under contaminated conditions [11]. Recent numerical work has also attempted to model adhesion enhancement induced by sand-particle breakage at the wheel–rail interface [12]. The above studies provide a solid physical basis for adhesion restoration analysis, but most performance comparisons still rely on peak adhesion, mean adhesion, recovery capacity or a limited number of characteristic cycles.

These conventional indicators are necessary but incomplete for dynamic braking assessment. Two curves may have similar maximum adhesion after recovery but substantially different low-adhesion duration, degradation severity, response delay or recovery intensity. Conversely, a curve with a high final adhesion level may still be unfavourable if it experiences a deep temporary loss or a long lag before recovery. Therefore, the evaluation target should be shifted from a single-point adhesion value to the entire disturbance–recovery process.

Resilience theory provides a suitable conceptual basis for this shift. The concept was originally formalised in ecology to describe a system's ability to absorb disturbance and maintain its functional structure [13]. It was later extended to community and infrastructure systems, where resilience is commonly measured by the degradation of a performance function and the time-dependent recovery of that function [14, 15]. In engineered systems, resilience-oriented design and resilience metrics emphasise absorptive, adaptive and recoverable capacities under disruptive events [16, 17]. Transportation studies further demonstrate that resilience can be quantified through time-dependent service performance and recovery processes, including waterway networks and mass railway transportation systems [18, 19]. These studies support the transfer of resilience thinking to wheel–rail adhesion, provided that the adhesion coefficient is explicitly treated as the system-performance variable.

The objective of this paper is therefore to formulate a dynamic adhesion-resilience metric for wheel–rail low-adhesion and recovery processes. The paper does not report new experiments. Instead, the proposed metric is demonstrated using digitised adhesion-recovery curves from two published studies. The wet-contact sanding curves reported by Omasta et al. are defined as Case 1, and the oil-contamination rolling-contact curves reported by Shi are defined as Case 2 [6, 11]. The contribution of this paper is a deterministic metric-calculation framework that supplements conventional maximum-adhesion evaluation and provides a quantitative basis for subsequent low-adhesion braking safety assessment.

2 Adhesion-resilience metric framework

2.1 Dynamic adhesion degradation and recovery process

In wheel–rail rolling contact, adhesion describes the ability of the contact interface to transmit tangential force under a normal load. The adhesion coefficient μ is commonly expressed as the ratio between the tangential traction or braking force and the corresponding normal wheel–rail contact force. It is therefore a direct performance variable for traction and braking, especially when the available adhesion approaches the demand imposed by the vehicle control system. Under low-adhesion contamination, however, μ is not a fixed material constant. It changes with creepage, surface state, contaminant distribution, particle entrainment and the temporal sequence of degradation and recovery.

Consequently, evaluating an adhesion-enhancement measure only by the maximum recovered adhesion coefficient is incomplete. Figure 1 gives a schematic illustration of three possible adhesion histories under comparable disturbance conditions. Curve 3 is clearly unfavourable because it recovers slowly and reaches a low post-recovery steady value. Curves 1 and 2, however, are not easily ranked by a single maximum value: Curve 1 recovers slowly but reaches a higher final level, whereas Curve 2 recovers faster but stabilises at a moderate level. This trade-off between recovery rapidity, recovery level and low-adhesion duration motivates the construction of an adhesion-resilience framework.

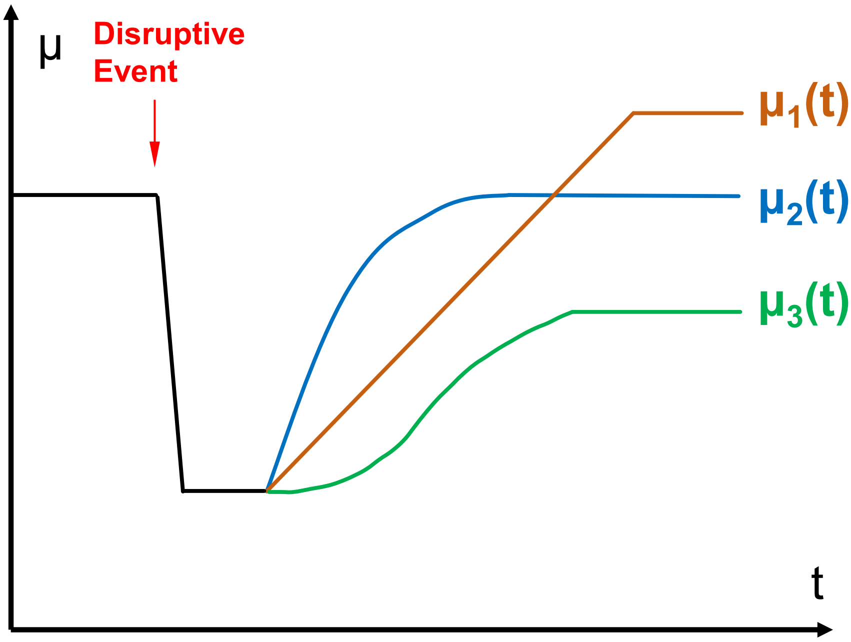

Figure 1: Schematic adhesion coefficient evolution curves under three operating conditions.

Let $\mu(x)$ denote the adhesion coefficient as a function of a process coordinate x. The horizontal coordinate of the present adhesion-resilience framework is not fixed to a single physical quantity. Instead, it is defined as a generalised process coordinate that describes the progress of the adhesion disturbance and recovery process. According to the available data and test configuration, x may be set as time, cycle number, number of revolutions or another equivalent monotonic process variable. In controlled braking tests or simulations with raw time histories, x can be directly set to time t; in twin-disc and rolling-contact data, x may be the cycle number N or the number of revolutions, provided that the equivalence relationship is stated explicitly.

Under normal circumstances, time as the horizontal coordinate in this framework is more intuitive. However, in the present literature-based case studies, both source curves use cycles as the horizontal coordinate. This does not invalidate the resilience formulation. For a rolling-contact test with constant rotational speed, the cycle number N and the elapsed time t satisfy

$$N = ft, \tag{1}$$

where f is the rotation frequency. Hence $dN = f\,dt$, and integrals and phase durations expressed in cycles differ from those expressed in time only by a constant scale factor. Because the reported resilience indices are normalised ratios, the use of cycles preserves the relative dynamic interpretation. If the rotational speed is not constant, the cycle coordinate should be converted through $N(t) = \int f(t)dt$ before direct comparison with time-domain braking responses. For generality, this paper retains x as the process coordinate in all formulae.

2.2 Phase-wise metrics

The adhesion evolution is divided into five phases, as illustrated in Figure 2: initial steady, degradation, lag, recovery and new steady. The initial steady phase represents the undisturbed or pre-event adhesion level μ_0. At x_0, the adhesion begins to deteriorate. The degradation phase ends at x_n, where the minimum adhesion level μ_n is reached. If the recovery mechanism does not act immediately, a lag phase may appear between x_n and x_r. The recovery phase extends from x_r to x_s, where the post-recovery steady level μ_s is reached.

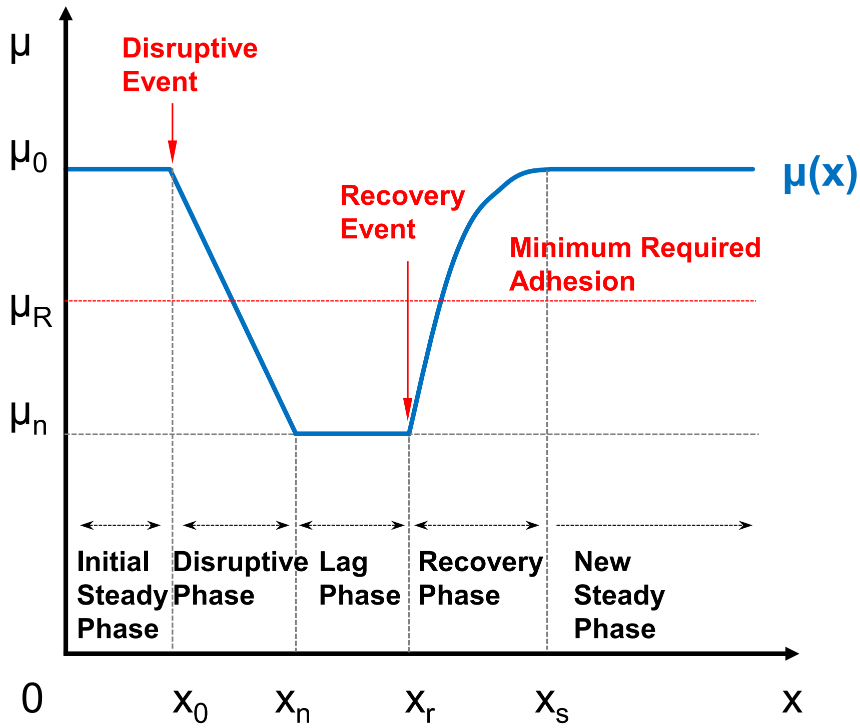

Figure 2: Phase division of the proposed adhesion-resilience framework with the generalised process coordinate x as the horizontal coordinate.

The metric construction follows the phase-wise resilience logic used in infrastructure resilience assessment: a system performance variable is first divided into steady, disruptive, recovery and new-steady phases, and the corresponding absorptive, adaptive and restorative capabilities are then quantified by complementary indicators rather than by a single capability alone [20]. In the present problem, the measurement of performance is the adhesion coefficient $\mu(x)$. The indicators are therefore designed to answer four questions: how severe the adhesion loss is, how long the contact remains in the low-adhesion state, how effectively the contact recovers, and how favourable the complete process is from a braking-safety perspective.

For the degradation phase, adhesion loss is defined as

$$AL = \int_{x_0}^{x_n} [\mu_0 - \mu(x)]\, dx. \tag{2}$$

AL is an area-type loss measure. It is larger when the adhesion drops deeper, remains low for a longer interval, or both. The mean rate of adhesion loss and the intensity of adhesion loss are defined as

$$RAL = \frac{\mu_0 - \mu_n}{x_n - x_0}, \qquad IAL = \frac{AL}{(\mu_0 - \mu_n)(x_n - x_0)}. \tag{3}$$

Here, RAL represents the average degradation slope between the onset of disturbance and the trough, whereas IAL describes the shape of the degradation trajectory relative to an idealised rectangular loss area. The lag duration is

$$RLT = x_r - x_n. \tag{4}$$

RLT is introduced because many adhesion-enhancement mechanisms do not become effective immediately after the minimum adhesion level is reached. A long lag implies that the braking system must operate under a low-adhesion constraint for a longer process interval even if the final adhesion level is eventually recovered.

For the recovery phase, adhesion gain is defined as

$$AG = \int_{x_r}^{x_s} [\mu(x) - \mu_r]\, dx, \tag{5}$$

where $\mu_r = \mu(x_r)$. AG is the cumulative adhesion gain during the recovery phase and is the recovery counterpart of AL. The mean recovery rate and recovery intensity are

$$RAG = \frac{\mu_s - \mu_r}{x_s - x_r}, \qquad IAG = \frac{AG}{(\mu_s - \mu_r)(x_s - x_r)}. \tag{6}$$

RAG quantifies the average recovery speed, while IAG reflects whether the recovery gain is concentrated early in the recovery interval or delayed toward the end. To compare different cases on a common scale, the following dimensionless indices are then used:

$$R = \frac{\mu_n}{\mu_0}, \tag{7}$$

where R is the robustness index. It measures the retained adhesion level at the trough and therefore represents the absorptive capability of the contact against the disturbance. Adhesion recovery ability is defined as

$$RAA = \frac{\mu_s - \mu_n}{\mu_0 - \mu_n}. \tag{8}$$

RAA evaluates the degree to which the adhesion loss from μ_0 to μ_n is compensated after recovery. Values close to unity indicate that the recovered steady level approaches the original baseline, whereas values below unity indicate incomplete recovery. The adhesion utilisation efficiency is defined by

$$\eta = \frac{\int_{x_0}^{x_s} \mu(x) dx}{\mu_0(x_s - x_0)}. \tag{9}$$

The efficiency index η is an integral measure over the entire disturbance–recovery interval. It penalises both deep adhesion degradation and long low-adhesion duration, which are directly relevant to braking safety. The relative recovery-rate and recovery-intensity factors are

$$\zeta_{rate} = \frac{RAG}{RAG + RAL}, \qquad \zeta_{intensity} = \frac{IAG}{IAG + IAL}. \tag{10}$$

These two factors normalise the recovery behaviour against the degradation behaviour so that a case with rapid and front-loaded recovery is favoured over a case with slow or delayed recovery. Finally, the temporal response factor is defined as

$$\tau = \frac{1}{1 + \exp\left[\frac{(x_s - x_r) - (x_n - x_0)}{x_s - x_0}\right]}. \tag{11}$$

The integrated adhesion-resilience index is calculated as the arithmetic mean of the six dimensionless components:

$$AR = \frac{1}{6}\left(R + RAA + \eta + \zeta_{rate} + \zeta_{intensity} + \tau\right). \tag{12}$$

A larger AR indicates a more favourable combination of low degradation, high recovery level, high utilisation efficiency, faster recovery, stronger recovery intensity and more favourable temporal response. The integrated index is not intended to replace the physical interpretation of the individual metrics; rather, it provides a compact ranking indicator for screening and comparison. The phase-wise definitions also make the framework auditable: if two cases obtain similar AR values, their individual components can still reveal whether the similarity originates from robustness, recovery completeness, recovery speed or process duration.

3 Literature-based case study and data processing

3.1 Source curves and digitisation

The proposed framework was evaluated using digitised curves from the two case groups defined in the Introduction. Case 1 corresponds to wet-contact sanding tests reported by Omasta et al., in which the contact was contaminated with water and different quantities of sand were supplied to the wheel–rail contact [11]. The two selected Case 1 curves are labelled C1-5g and C1-15g, where 5 g and 15 g denote the sand quantity used in the corresponding wet-contact sanding tests. Case 2 corresponds to oil-contamination rolling-contact tests reported by Shi [6]. The four selected Case 2 curves are labelled C2-10μL, C2-20μL, C2-30μL and C2-40μL, where 10, 20, 30 and 40 μL denote the oil quantity used to generate the corresponding low-adhesion condition.

The digitised data are used only to demonstrate the metric calculation procedure. No new experimental measurements are claimed in this paper. Direct cross-platform ranking between Case 1 and Case 2 is avoided because the test rigs, materials, contaminants and operating conditions differ. Comparisons are made within each case group, while cross-group results are used to examine the applicability of the metric framework to different curve shapes.

The Case 1 curves in Figure 3 provide a wet-contact sanding example. In this paper, C1-5g denotes the wet-contact sanding curve obtained with 5 g of sand, whereas C1-15g denotes the corresponding curve obtained with 15 g of sand. These two sand-quantity cases have similar initial adhesion levels, but they differ in the depth of the short-term adhesion reduction and in the post-recovery level. This indicates that sand quantity affects not only the final adhesion level but also the transient degradation–recovery trajectory.

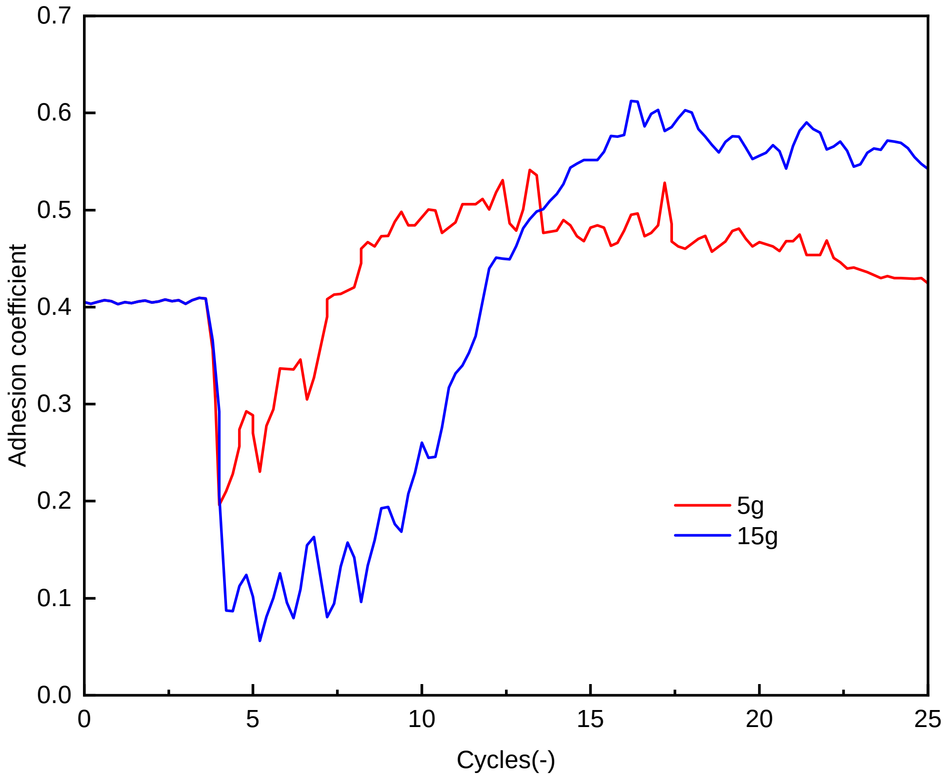

Figure 3: Digitised and re-plotted adhesion recovery curves for Case 1 under wet-contact sanding conditions.

The Case 2 oil-contamination curves in Figure 4 provide an oil-quantity example. In this paper, C2-10μL, C2-20μL, C2-30μL and C2-40μL denote oil-contamination curves obtained with 10, 20, 30 and 40 μL of oil, respectively. These curves show that the low-adhesion duration and recovery trajectory depend strongly on oil quantity. Although the final adhesion levels of the Case 2 oil-contamination curves are all close to the initial high-adhesion range, the process coordinate required for recovery increases substantially as the oil quantity increases. This behaviour is consistent with the physical expectation that a larger contaminant quantity prolongs the low-adhesion state.

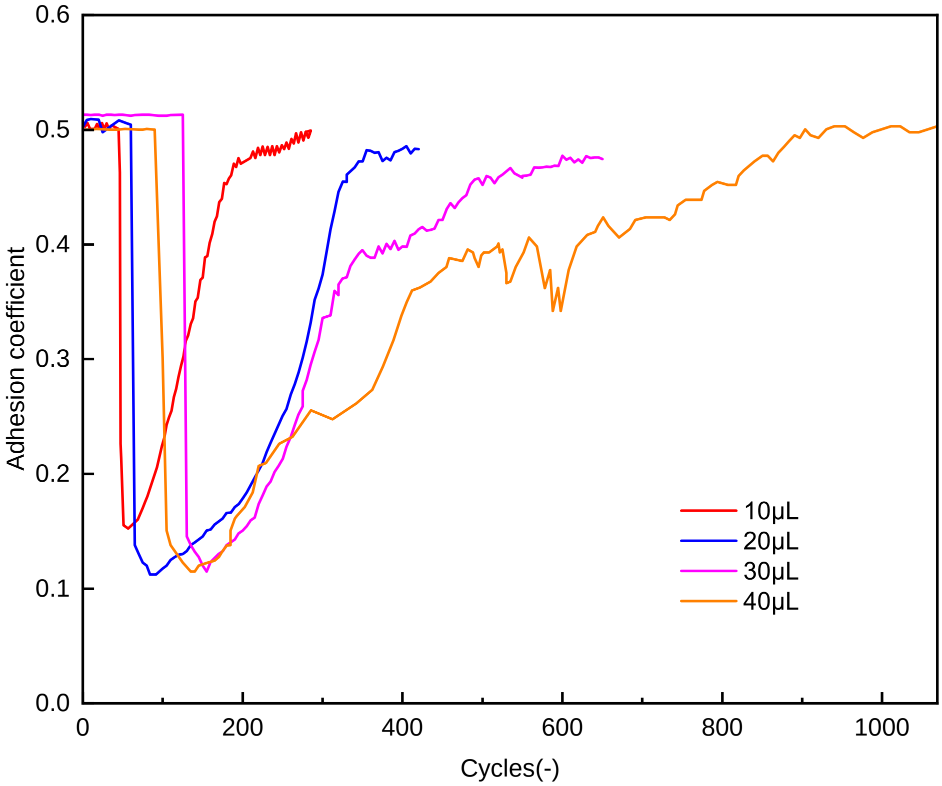

Figure 4: Digitised and re-plotted adhesion coefficient curves for Case 2 under oil-contaminated wheel–rail rolling contact.

Table 1 summarises the six digitised curves used in the demonstration. Case 1 contains two wet-contact sanding curves with different sand quantities, whereas Case 2 contains four oil-contamination curves with different oil quantities. The table is included to make the correspondence between case labels, source curves, media, control variables and test conditions explicit before the metric calculation is reported.

Case	Case group	Original figure	Medium	Variable	Condition
C1-5g	Case 1	Fig. 9	Water	Sand quantity	5 g sand in wet contact
C1-15g	Case 1	Fig. 9	Water	Sand quantity	15 g sand in wet contact
C2-10μL	Case 2	Fig. 3-4	Oil	Oil quantity	10 μL oil contamination
C2-20μL	Case 2	Fig. 3-4	Oil	Oil quantity	20 μL oil contamination
C2-30μL	Case 2	Fig. 3-4	Oil	Oil quantity	30 μL oil contamination
C2-40μL	Case 2	Fig. 3-4	Oil	Oil quantity	40 μL oil contamination

Table 1: Digitised literature-based case studies used for adhesion-resilience metric demonstration.

3.2 Characteristic-point identification

A deterministic rule-based procedure was used to identify x_0, x_n, x_r and x_s. To avoid the displacement of abrupt features caused by smoothing across phase boundaries, characteristic points were identified from the raw cleaned digitised curve. After the phase boundaries were determined, the curve was smoothed only within each phase, and the phase-wise smoothed curve was then used for the integral-type metrics. This processing sequence preserves the rapid drop near the disturbance point while still reducing local digitisation noise during metric calculation.

For the present literature-based cases, the lag phase was treated according to the observed degradation–recovery characteristics of each curve. Because the recovery trend started immediately after the adhesion trough in the six digitised curves, x_n and x_r were set to the same characteristic point, namely $x_r = x_n$ and $RLT = 0$. This treatment avoids introducing an artificial lag interval from local fluctuations after the minimum point.

Figure 5 illustrates the characteristic-point identification using the C2-30μL curve, namely the Case 2 oil-contamination curve obtained with 30 μL of oil. The uploaded node plot marks $x_0 = 125$, $x_n = x_r = 155$ and $x_s = 505$, showing that the lag phase is not imposed for this curve because the recovery phase starts from the performance trough. This example is used only to visualise the node-identification result; the full set of calculated characteristic points is listed in Table 2.

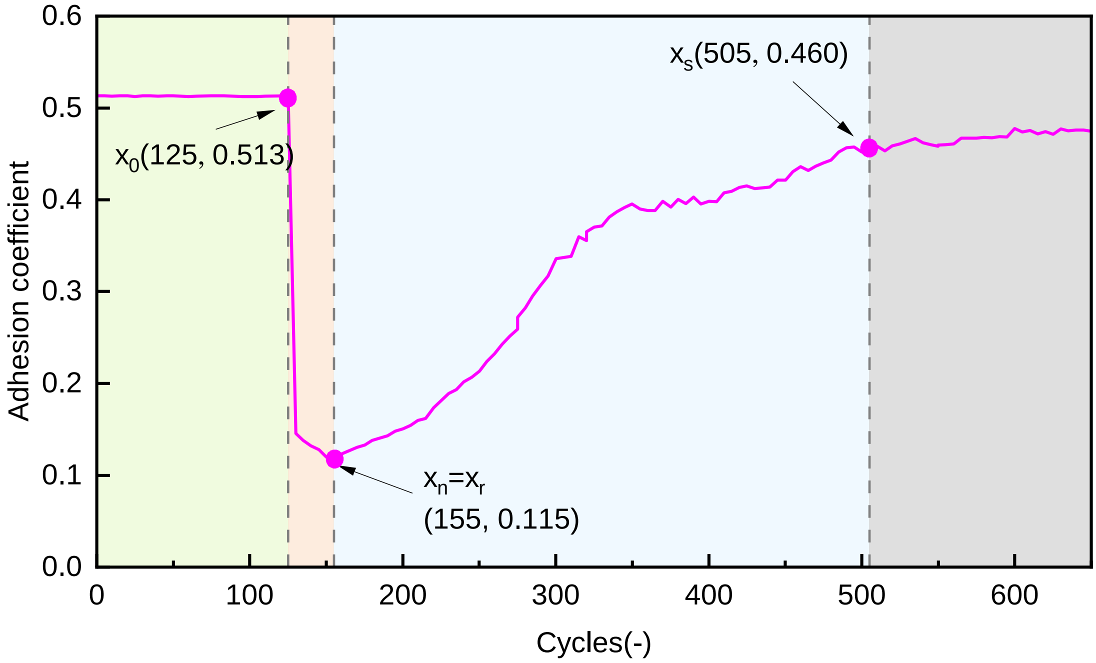

Figure 5: Characteristic-point identification for the Case 2 30 μL oil-contamination curve.

Case	x_0	x_n	x_r	x_s	μ_0	μ_n	μ_r	μ_s
C1-5g	3.60	4.00	4.00	11.00	0.406	0.196	0.196	0.504
C1-15g	3.60	5.20	5.20	15.80	0.406	0.056	0.056	0.592
C2-10μL	35.90	56.90	56.90	209.80	0.503	0.152	0.152	0.480
C2-20μL	60.10	84.30	84.30	350.10	0.505	0.112	0.112	0.478
C2-30μL	125.00	155.00	155.00	505.00	0.513	0.115	0.115	0.460
C2-40μL	90.06	135.09	135.09	890.24	0.500	0.115	0.115	0.498

Table 2: Automatically identified characteristic points and adhesion levels. The coordinate x denotes the original cycle-based process coordinate retained from the digitised source curves; the 30 μL case is visualised in Figure 5.

4 Results and discussion

4.1 Maximum adhesion versus adhesion-resilience metrics

Table 3 and Figure 6 show that the maximum adhesion coefficient and the integrated adhesion-resilience index do not always provide the same interpretation. For example, the C1-15g curve, corresponding to the wet-contact sanding test with 15 g of sand, has the highest maximum adhesion coefficient, but its AR is lower than that of the C1-5g curve, corresponding to the wet-contact sanding test with 5 g of sand, because it has a much lower robustness value and a lower utilisation efficiency. Similarly, the Case 2 oil-contamination curves, corresponding to 10–40 μL oil quantities, have similar maximum adhesion coefficients after recovery, whereas their AR values differ because their degradation depths, recovery durations and temporal response factors are different. These results support the main premise of the paper: the maximum adhesion coefficient should be supplemented by a dynamic process-based metric when low-adhesion braking safety is assessed.

Case	μ_{max}	R	η	RAA	ζ_{rate}	$\zeta_{intensity}$	τ	AR
C1-5g	0.514	0.483	0.946	1.469	0.077	0.625	0.291	0.649
C1-15g	0.602	0.138	0.714	1.534	0.188	0.412	0.324	0.552
C2-10μL	0.506	0.303	0.643	0.934	0.114	0.515	0.319	0.471
C2-20μL	0.508	0.222	0.476	0.931	0.078	0.322	0.303	0.389
C2-30μL	0.513	0.224	0.603	0.868	0.069	0.428	0.301	0.415
C2-40μL	0.503	0.230	0.677	0.993	0.056	0.452	0.292	0.450

Table 3: Calculated maximum adhesion and adhesion-resilience metrics.

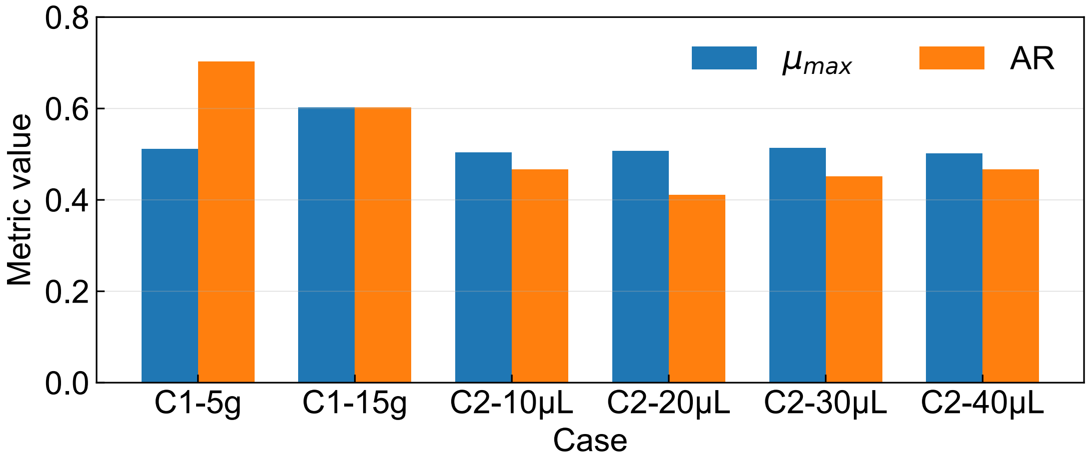

Figure 6: Comparison between maximum adhesion coefficient and the integrated adhesion-resilience index.

4.2 Implications for low-adhesion braking safety assessment

From a braking-control perspective, a low maximum adhesion value directly limits the available braking force. However, the temporal evolution of adhesion is also important. A long low-adhesion duration can increase the demand on wheel slide protection and may prolong the period in which braking force must be reduced. Conversely, rapid recovery can increase the available adhesion margin earlier in the braking event. The proposed AR index and its components therefore provide a compact but interpretable way to evaluate low-adhesion recovery curves for braking safety, antiskid control and future sanding-strategy assessment.

5 Conclusions and contributions

This paper proposed an adhesion-resilience framework for dynamic wheel–rail adhesion degradation and recovery. The main conclusions are as follows.

First, the wheel–rail adhesion process can be decomposed into initial steady, degradation, lag, recovery and new steady phases. This decomposition enables adhesion behaviour to be evaluated as a dynamic process rather than only through a peak or steady value.

Second, the proposed metric set quantifies robustness, adhesion recovery ability, adhesion utilisation efficiency, recovery rate, recovery intensity and temporal response. These components are combined into an integrated adhesion-resilience index AR, while still allowing physical interpretation of individual degradation and recovery mechanisms.

Third, the two literature-based case groups show that AR can distinguish recovery behaviours that are not fully captured by the maximum adhesion coefficient. In particular, cases with similar maximum adhesion levels can have different low-adhesion duration, recovery rate and integrated resilience.

Fourth, because the source curves use cycles as their horizontal coordinate, a process-coordinate formulation was adopted. Under constant-speed rolling, cycle count is linearly proportional to elapsed time, so the normalised metrics retain their dynamic interpretation. Future work should apply the same framework to controlled twin-disc or full-scale braking tests with raw time histories, repeated trials and uncertainty quantification.

Acknowledgements

This work was supported by the National Key Research and Development Program of China (2024YFB4303300), Science and Technology Research and Development Programme Topics of China State Railway Group Co., Ltd. (P2023J040-4), and Shanghai Collaborative Innovation Research Center for Multi-network & Multi-model Rail Transit. The corresponding author of this paper is Prof. Jianyong Zuo.

References

[1] Kalker J. J., Three-Dimensional Elastic Bodies in Rolling Contact, Kluwer Academic Publishers, Dordrecht, 1990.

[2] Polach O., "Creep forces in simulations of traction vehicles running on adhesion limit", Wear, 258(7–8): 992–1000, 2005. doi: 10.1016/j.wear.2004.03.046.

[3] Olofsson U., Zhu Y., Abbasi S., Lewis R., Lewis S., "Tribology of the wheel–rail contact: aspects of wear, particle emission and adhesion", Vehicle System Dynamics, 51(7): 1091–1120, 2013. doi: 10.1080/00423114.2013.800215.

[4] Beagley T. M., Pritchard C., "Wheel/rail adhesion–the overriding influence of water", Wear, 35(2): 299–313, 1975. doi: 10.1016/0043-1648(75)90078-2.

[5] Li Z., Arias-Cuevas O., Lewis R., Gallardo-Hernandez E. A., "Rolling–Sliding Laboratory Tests of Friction Modifiers in Leaf Contaminated Wheel–Rail Contacts", Tribology Letters, 33(2): 97–109, 2009. doi: 10.1007/s11249-008-9393-3.

[6] Shi L. B., Study on the Adhesion Enhancement and Damage Behaviours of Wheel/Rail in the Application of Hard Particles, Ph.D. dissertation, Southwest Jiaotong University, Chengdu, 2020. doi:10.27414/d.cnki.gxnju.2020.002527.

[7] Skipper W. A., Chalisey A., Lewis R., "A review of railway sanding system research: adhesion restoration and leaf layer removal", Tribology: Materials, Surfaces and Interfaces, 12(4): 237–251, 2018. doi: 10.1080/17515831.2018.1542791.

[8] Arias-Cuevas O., Li Z., Lewis R., Gallardo-Hernandez E. A., "Rolling–sliding laboratory tests of friction modifiers in dry and wet wheel–rail contacts", Wear, 268(3–4): 543–551, 2010. doi: 10.1016/j.wear.2009.09.015.

[9] Arias-Cuevas O., Li Z., Lewis R., "Investigating the lubricity and electrical insulation caused by sanding in dry wheel–rail contacts", Tribology Letters, 37(3): 623–635, 2010. doi: 10.1007/s11249-009-9560-1.

[10] Lewis R., Dwyer-Joyce R. S., "Wear at the wheel/rail interface when sanding is used to increase adhesion", Proceedings of the Institution of Mechanical Engineers, Part F: Journal of Rail and Rapid Transit, 220(1): 29–41, 2006. doi: 10.1243/095440905X33260.

[11] Omasta M., Machatka M., Smejkal D., Hartl M., Krupka I., "Influence of sanding parameters on adhesion recovery in contaminated wheel–rail contact", Wear, 322–323: 218–225, 2015. doi: 10.1016/j.wear.2014.11.017.

[12] Zhang B., Nadimi S., Lewis R., "Modelling the adhesion enhancement induced by sand particle breakage at the wheel–rail interface", Wear, 538–539: 205232, 2024. doi: 10.1016/j.wear.2023.205232.

[13] Holling C. S., "Resilience and Stability of Ecological Systems", Annual Review of Ecology and Systematics, 4: 1–23, 1973. doi: 10.1146/annurev.es.04.110173.000245.

[14] Cutter S. L., Barnes L., Berry M., Burton C., Evans E., Tate E., Webb J., "A place-based model for understanding community resilience to natural disasters", Global Environmental Change, 18(4): 598–606, 2008. doi:

10.1016/j.gloenvcha.2008.07.013.
[15] Bruneau M., Chang S. E., Eguchi R. T., Lee G. C., O'Rourke T. D., Reinhorn A. M., Shinozuka M., Tierney K., Wallace W. A., von Winterfeldt D., "A Framework to Quantitatively Assess and Enhance the Seismic Resilience of Communities", Earthquake Spectra, 19(4): 733–752, 2003. doi: 10.1193/1.1623497.
[16] Youn B. D., Hu C., Wang P., "Resilience-Driven System Design of Complex Engineered Systems", Journal of Mechanical Design, 133(10): 101011, 2011. doi: 10.1115/1.4004981.
[17] Francis R., Bekera B., "A metric and frameworks for resilience analysis of engineered and infrastructure systems", Reliability Engineering & System Safety, 121: 90–103, 2014. doi: 10.1016/j.ress.2013.07.004.
[18] Baroud H., Barker K., Ramirez-Marquez J. E., Rocco C. M., "Importance measures for inland waterway network resilience", Transportation Research Part E: Logistics and Transportation Review, 62: 55–67, 2014. doi: 10.1016/j.tre.2013.11.010.
[19] Adjetey-Bahun K., Birregah B., Chatelet E., Planchet J. L., "A model to quantify the resilience of mass railway transportation systems", Reliability Engineering & System Safety, 153: 1–14, 2016. doi: 10.1016/j.ress.2016.03.015.
[20] Nan C., Sansavini G., "A quantitative method for assessing resilience of interdependent infrastructures", Reliability Engineering & System Safety, 157: 35–53, 2017. doi: 10.1016/j.ress.2016.08.013.